Sequence Impedance Measurement of Utility-Scale Wind Turbines and Inverters – Reference Frame, Frequency Coupling, and MIMO/SISO Forms

Shahil Shah , *Senior Member, IEEE*, Przemyslaw Koralewicz , *Member, IEEE*, Vahan Gevorgian , *Senior Member, IEEE*, and Robb Wallen

Abstract—Sequence impedance responses are increasingly used for the stability analysis of converter-grid systems; however, many aspects of the sequence impedance measurement process, particularly those resulting from the frequency coupling between the positive- and negative-sequence impedances, are not yet fully explored. Existing methods for measuring sequence impedance with frequency coupling are complicated, not suitable for large wind turbines and inverters, and they can measure the sequence impedance in only one of the MIMO and SISO forms. This paper shows that the sequence impedance has a reference frame similar to the dq impedance and presents a method for measuring the sequence impedance with frequency coupling. The proposed method aligns the sequence impedance reference frame based on the estimation of the grid voltage angle and obtains the impedance response in both MIMO and SISO forms. The paper also demonstrates the impact of the fundamental frequency on the accuracy of the impedance measurements. The proposed method and practical issues associated with the impedance measurement of utility-scale wind turbines and inverters are demonstrated on a 1.9-MW Type III wind turbine and a 2.2-MVA inverter using an impedance measurement system built around a 7-MW/13.8-kV grid simulator and a 5-MW dynamometer.

Index Terms—Impedance measurement, sequence impedance, dq impedance, stability analysis, control interactions, resonance, subsynchronous oscillations.

I. INTRODUCTION

IMPEDANCE-BASED analysis has become the mainstream approach for the stability analysis of converter-grid systems—including wind and solar power plants, microgrids, electric traction systems—and high-voltage dc transmission networks [1]–[8]. Certain utilities have started demanding that vendors provide the impedance response data of wind turbines and inverters to support system stability studies [9]–[11]. Impedance responses can also be used to validate the dynamic performance of electromagnetic transient simulation models over a broad frequency range. These developments have made the impedance measurement of utility-scale wind turbines and inverters an important grid integration test.

The impedance-based stability analysis method for three-phase power systems was initially developed by modeling these systems in a synchronously rotating dq reference frame [12]. The impedance in the dq frame is a two-by-two transfer matrix. At least two perturbation tests are required to measure the dq impedance [13]–[15]. The dq impedance measurement also requires that the dq reference frame is aligned with the grid voltage angle [16]; the latter is obtained by either FFT analysis of the voltage measurements or by using a phase-locked loop (PLL). The FFT approach assumes that the fundamental frequency is fixed at its nominal value, which could result in significant errors. On the other hand, the PLL approach causes errors because of the effect of the injected perturbations on the PLL output; these errors can be minimized, however, by using either a very low-bandwidth PLL or a compensation method [17], [18].

Different from the dq impedance approach, [19] proposed the use of positive- and negative-sequence impedance responses for the stability analysis of three-phase systems. It was initially observed that the positive- and negative-sequence impedance responses of wind turbines and inverters are uncoupled for balanced operating conditions, which enables stability analysis using the Nyquist criteria for single-input single-output (SISO) systems and Bode plots instead of requiring the more complicated generalized Nyquist criteria required for the multi-input multi-output (MIMO) systems [20]. Recent works, however, have discovered that the sequence impedances of three-phase active devices—wind turbines, inverters, high-voltage dc converters, synchronous generators, etc.—are coupled because of the frequency coupling effects [21]–[25]. The frequency coupling in power converters is caused by PLLs, dc-bus voltage control, asymmetric implementation of the d- and q-axis controls, and control functions acting on phasor variables such as the magnitude and frequency of voltages and the active and reactive power output [21], [25]–[28]. The frequency coupling in synchronous generators, on the other hand, is caused by power system stabilizers and the saliency of the machine dynamics in addition to the power, frequency, and voltage control loops [29]. The frequency coupling between the sequence impedances is generally

dominant only at low frequencies less than a couple hundred hertz [21], [30], [31]; hence, high-frequency stability problems can be analysed using uncoupled positive- and negative-sequence impedance responses ignoring the frequency coupling. The analysis of stability problems at frequencies less than a couple hundred hertz, such as system wide subsynchronous oscillations because of control interactions among inverter-based resources in different parts of the grid [7]–[9], must consider the frequency coupling in the sequence impedance responses.

Most existing works on sequence impedance measurement ignore the frequency coupling between the positive- and negative-sequence impedance responses [32]–[34]. Refs. [21]–[25] measured the sequence impedance including frequency coupling in simulations, which bypasses many problems encountered during experimental measurements. Ref. [35] presented a method to experimentally measure the sequence impedance with frequency coupling of a grid-connected inverter. The authors represented the sequence impedance of the inverter by uncoupled positive- and negative-sequence SISO impedances that are dependent on the grid impedance. As elaborated in this paper, stability analysis using the grid dependent SISO sequence impedances is possible only for certain applications. Moreover, the SISO representation of the sequence impedance with frequency coupling cannot be used to aggregate the impedance responses of multiple components in a system, such as wind turbines in a wind power plant. The impedance measurement method presented in [35] requires three perturbation tests, each with a different value of the grid/source impedance, making the measurement process highly complicated and not feasible for large, utility-scale wind turbines and inverters. Changing the grid or source impedance for each perturbation test might also disturb the operation point. Ref. [36] demonstrated admittance measurement of a power converter in a stationary $\alpha\beta$ frame, which is related to but not the same as the sequence admittance. Moreover, the measurements were performed only up to 190 Hz. One major challenge in measuring the sequence admittance with frequency coupling is the presence of a nonzero voltage component at the coupling frequency—it appears because of the coupling frequency response in currents and the non-negligible impedance of the electrical network at the terminals of the device under test (DUT). Refs. [37] and [38] proposed the active cancellation of the coupling frequency component in voltages by using a control loop in the perturbation source. This, however, unnecessarily increases the complexity of the measurement process, and the accuracy of the measured responses becomes dependent on the effectiveness of the active control loop. Above all, none of the existing works demonstrate the impedance measurement of utility-scale wind turbines and inverters and discuss the associated practical issues.

This discussion shows that the fundamental theory for measuring the sequence impedance with frequency coupling is not yet fully developed. On the other hand, [21]–[23] showed that the sequence impedance with frequency coupling is mathematically equivalent to the dq impedance. This raises questions such as whether the sequence impedance is also associated with a reference frame, whether the sequence impedance measurement also requires at least two sets of linearly independent perturbation tests, whether the estimation of the grid voltage angle is

important for the sequence impedance measurement, whether the value of the fundamental frequency during the impedance measurement impacts the measurement accuracy, and whether it is possible to measure the sequence impedance with frequency coupling without active cancellation of the coupling frequency component in the three-phase voltages. This paper answers these questions and presents a method for measuring sequence impedance with frequency coupling. The paper shows that the sequence impedance measurement faces the same challenges as the dq impedance measurement. The main contributions of this paper are as follows:

1) The paper presents a method for measuring sequence impedance with frequency coupling. It uses two sets of linearly independent perturbation tests. Unlike the existing methods, the proposed method does not require cancellation of the coupling frequency component in voltages or a different grid/source impedance for each perturbation test.

2) The paper presents the relationship between the MIMO and SISO forms of the sequence impedance with frequency coupling and demonstrates the derivation of the sequence impedance response for the SISO form using measurements obtained for the MIMO form.

3) The paper shows that the sequence impedance of three-phase active devices—power converters, synchronous generators, etc.—has a reference frame. It is also shown that the sequence impedance reference frame is related with the dq impedance reference frame.

4) The paper demonstrates the alignment of the sequence impedance reference frame by an FFT analysis approach, which assumes the fundamental frequency to be fixed at 60 Hz. The paper experimentally demonstrates the impact of this assumption on the measurement accuracy.

5) The paper demonstrates the proposed method and practical problems associated with the sequence impedance measurement of utility-scale wind turbines and inverters on a 1.9-MW wind turbine and a 2.2-MVA inverter over a broad frequency range, from 0.1 Hz to 1 kHz, using an impedance measurement system built around a 7-MW/13.8-kV grid simulator; a 5-MW dynamometer; and a medium-voltage, GPS-synchronized measurement and data acquisition system. To the best of the authors' knowledge, this paper demonstrates for the first time the impedance measurement of utility-scale wind turbines and inverters.

6) The paper experimentally validates the relationship between the dq and sequence admittances by comparing the dq admittance of a 1.9-MW wind turbine obtained by direct measurement with those derived from the sequence admittance measurements, thereby invalidating concerns raised in [39] on the validity of the relationship between the dq and sequence impedance/admittance models.

The rest of the paper is organized as follows: Section II presents the MIMO and SISO forms of the sequence admittance with frequency coupling. Section III shows that the sequence admittance has a reference frame and presents an algorithm to align the reference frame with the grid voltage angle. Section IV presents a method for measuring the sequence admittance with frequency coupling. Section V validates the proposed

method using numerical simulations and analytical models of a grid-connected voltage source converter (VSC). Section VI experimentally demonstrates the method on a utility-scale wind turbine and an inverter. Section VII concludes this paper.

II. SEQUENCE ADMITTANCE WITH FREQUENCY COUPLING

A. MIMO Form

As shown in [21], three-phase active devices generally exhibit a frequency-coupled response because of the time-periodic nature of their dynamics: the injection of a positive-sequence voltage perturbation at a frequency, e.g., f_p, produces a negative-sequence response at frequency f_p-2f_1 in currents in addition to the positive-sequence response at frequency f_p. A similar frequency-coupled response is present in currents for the injection of a negative-sequence voltage perturbation. Sequence admittance with frequency coupling can be defined as follows [21]–[23]:

$$\begin{bmatrix} I_p(s+j\omega_1) \\ I_n(s-j\omega_1) \end{bmatrix} = \begin{bmatrix} Y_{\mathrm{pp}}(s) & Y_{\mathrm{pn}}(s) \\ Y_{\mathrm{np}}(s) & Y_{\mathrm{nn}}(s) \end{bmatrix} \begin{bmatrix} V_p(s+j\omega_1) \\ V_n(s-j\omega_1) \end{bmatrix} \quad (1)$$

where subscripts p and n, respectively, denote the positive- and negative-sequence components of three-phase voltages and currents. The sequence admittance matrix in (1) is denoted by $\mathbf{Y}_{\mathrm{PN}}(s)$. This MIMO representation is the most general form of the sequence admittance with frequency coupling.

The sequence admittance with frequency coupling can also be represented using four scalar transfer functions:

$$\left.\begin{array}{l} Y_p(s) = \frac{I_p(s)}{V_p(s)} \\ Y_{\mathrm{cp}}(s) = \frac{I_n(s-j2\omega_1)}{V_p(s)} \end{array}\right\} \text{where} V_n(s-j2\omega_1) = 0 \quad (2)$$

$$\left.\begin{array}{l} Y_n(s) = \frac{I_n(s)}{V_n(s)} \\ Y_{\mathrm{cn}}(s) = \frac{I_p(s+j2\omega_1)}{V_n(s)} \end{array}\right\} \text{where} V_p(s+j2\omega_1) = 0 \quad (3)$$

where $Y_p(s)$ and $Y_n(s)$, respectively, denote the standard positive- and negative-sequence admittances; and $Y_{\mathrm{cp}}(s)$ and $Y_{\mathrm{cn}}(s)$ denote, respectively, the transfer functions from the injected positive- and negative-sequence voltage perturbations to the response in the currents at the coupling frequency. The transfer functions in (2) and (3) are related to the elements of $\mathbf{Y}_{\mathrm{PN}}(s)$ as follows:

$$Y_p(s) = Y_{\mathrm{pp}}(s-j\omega_1) Y_{\mathrm{cp}}(s) = Y_{\mathrm{np}}(s-j\omega_1)$$
$$Y_n(s) = Y_{\mathrm{nn}}(s+j\omega_1) Y_{\mathrm{cn}}(s) = Y_{\mathrm{pn}}(s+j\omega_1) \quad (4)$$

Although the four scalar transfer functions defined in (2) and (3) are mathematically identical to the elements of the transfer matrix defined in (1), it quickly becomes intractable to handle the sequence admittances of multiple components in a network when they are represented using the scalar transfer functions; however, the representation of the sequence admittance with frequency coupling using the four scalar transfer functions is more intuitive for comparing the coupling admittances, $Y_{\mathrm{cp}}(s)$ and $Y_{\mathrm{cn}}(s)$, against the conventional positive- and negative-sequence admittances, $Y_p(s)$ and $Y_n(s)$, for determining when the frequency coupling in the sequence admittance can be ignored.
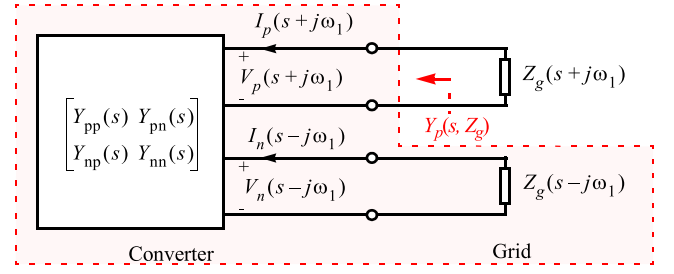

Fig. 1. Small-signal representation of a converter-grid system when the sequence impedance of the grid does not exhibit frequency coupling.

B. SISO Form

The sequence components of three-phase voltages and currents at the terminals of a three-phase equipment can be related depending on the impedance of the grid at its terminals as follows:

$$V_p(s) = -I_p(s) \cdot Z_g(s)$$
$$V_n(s) = -I_n(s) \cdot Z_g(s) \quad (5)$$

where $Z_g(s)$ is the grid impedance. Substituting (5) in (1), the sequence admittance with frequency coupling of the equipment can be represented using two SISO transfer functions—uncoupled positive- and negative-sequence admittances—that are dependent on the grid impedance $Z_g(s)$:

$$Y_p(s, Z_g) = Y_{\mathrm{pp}}(s-j\omega_1)- \frac{Y_{\mathrm{pn}}(s-j\omega_1) Y_{\mathrm{np}}(s-j\omega_1) \cdot Z_g(s-j2\omega_1)}{1 + Y_{\mathrm{nn}}(s-j\omega_1) \cdot Z_g(s-j2\omega_1)} \quad (6)$$

$$Y_n(s, Z_g) = Y_{\mathrm{nn}}(s+j\omega_1)- \frac{Y_{\mathrm{pn}}(s+j\omega_1) Y_{\mathrm{np}}(s+j\omega_1) \cdot Z_g(s+j2\omega_1)}{1 + Y_{\mathrm{nn}}(s+j\omega_1) \cdot Z_g(s+j2\omega_1)} \quad (7)$$

This SISO representation considerably simplifies the stability analysis because it supports the use of the simple Nyquist criteria and Bode plots for the analysis instead of requiring the generalized Nyquist criteria for the MIMO systems; however, the SISO representation is valid only if the grid or the source network does not exhibit frequency coupling in its sequence impedance, i.e., when the relations in (5) are valid. In other words, such a representation is valid if the small-signal dynamics of a converter-grid system can be represented as shown in Fig. 1. Note that the SISO representation is not suitable for aggregating the sequence admittances of different components in a network.

III. REFERENCE FRAME OF SEQUENCE ADMITTANCE

The sequence admittance elements that capture the frequency coupling—$Y_{\mathrm{pn}}(s)$ and $Y_{\mathrm{np}}(s)$ in (1), and $Y_{\mathrm{cp}}(s)$ and $Y_{\mathrm{cn}}(s)$ in (2) and (3)—represent gains between the voltage and current perturbations at different frequencies. The difference between the frequencies of the voltage and current perturbations in the definitions of these coupling admittances is $2\omega_1$ rad/s (i.e., $2f_1$ in Hz). Because of this frequency difference, when the data
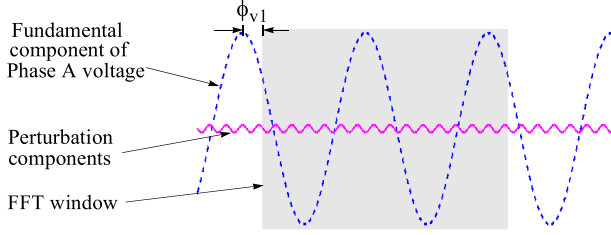
Fig. 2. Graphic representation of the waveform of the Phase A voltage showing the relative position of an FFT window with respect to the fundamental frequency component.

Fig. 3. Steps for measuring sequence admittance with frequency coupling by using two perturbation tests and a reference frame alignment algorithm.

window used for the FFT analysis slides over time, the phase of the voltage and current perturbations will change at different rates, which makes the phase of the coupling admittances time dependent. Moreover, because the frequency difference is $2f_1$, the phase of the coupling admittances varies with time in a periodic manner with the period of $(2f_1)^{-1}$. Hence, to obtain a meaningful response of the coupling admittances, they should be measured such that the data captures used for the FFT analysis for all perturbation tests align with the same point on wave of the fundamental components of the three-phase voltages. In other words, the phase responses of the coupling admittances depend on the starting point of the data window used for the FFT analysis with respect to the fundamental component of the Phase A voltage, i.e., on angle ϕ_{v1}, defined in Fig. 2 [31]. Section VI shows that keeping ϕ_{v1} zero during the sequence admittance measurement is equivalent to aligning the d-axis of the dq reference frame with the Phase A voltage during the dq admittance measurement.

The moving data window used for the FFT analysis basically defines the reference frame of the sequence admittance, and it should be aligned with the grid voltage angle. This can be achieved as follows. The Fourier component of a variable at an arbitrary frequency, f, when the FFT data window aligns such that ϕ_{v1} is zero can be related with the same Fourier component when ϕ_{v1} has a nonzero value, e.g., α:

$$\boldsymbol{X}[f]|_{\phi_{v1}=0} = \boldsymbol{X}[f]|_{\phi_{v1}=\alpha} \cdot e^{-j\left(\frac{f}{f_1} \cdot \alpha\right)} \tag{8}$$

$$\boldsymbol{Y}_{\mathrm{PN}}(s) = \begin{bmatrix} I_p(s+j\omega_1)_{(1)} & I_p(s+j\omega_1)_{(2)} \\ I_n(s-j\omega_1)_{(1)} & I_n(s-j\omega_1)_{(2)} \end{bmatrix}$$
$$\cdot \begin{bmatrix} V_p(s+j\omega_1)_{(1)} & V_p(s+j\omega_1)_{(2)} \\ V_n(s-j\omega_1)_{(1)} & V_n(s-j\omega_1)_{(2)} \end{bmatrix}^{-1} \tag{9}$$

Eq. (8) can be used to compensate for the phase of the Fourier components so that all of them align with the grid voltage angle.

IV. MEASUREMENT OF SEQUENCE ADMITTANCE

A. Impact of Finite Grid or Source Impedance

The independent measurement of the elements of $\boldsymbol{Y}_{\mathrm{PN}}(s)$ by separately injecting positive- and negative-sequence perturbations requires that the voltage perturbation at the coupling frequency stays at zero. It is difficult to ensure this condition
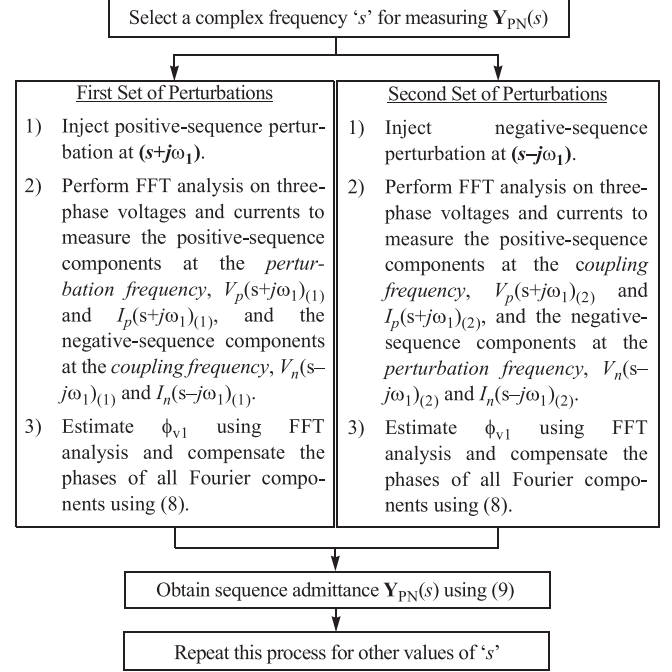
because of the finite impedance of the electrical network at the terminals of the DUT. This problem is similar to the existence of a nonzero q-axis component in three-phase voltages when a perturbation is injected in the d-axis, or vice versa, to measure the dq admittance response. The problem is solved for the dq admittance measurement by using two sets of linearly independent perturbation tests [17]. This paper proposes a similar approach for measuring sequence admittance with frequency coupling by using two perturbation tests.

B. Measurement of MIMO Sequence Admittance

The flowchart shown in Fig. 3 describes the process of measuring the sequence admittance matrix, $\boldsymbol{Y}_{\mathrm{PN}}(s)$, by using two perturbation tests. For each value of the complex frequency 's', two tests are conducted by injecting, respectively, a positive-sequence perturbation at frequency $(s+j\omega_1)$ and a negative-sequence perturbation at frequency $(s-j\omega_1)$. The measurement process is further streamlined using the fact that the injection of a negative-sequence perturbation at frequency $(s-j\omega_1)$ is equivalent to the injection of a positive-sequence perturbation at frequency $(-s+j\omega_1)$ [21]; hence, for each value of the complex frequency 's', two perturbation tests are conducted by injecting a positive-sequence perturbation, respectively, at frequencies $(s+j\omega_1)$ and $(-s+j\omega_1)$. For both tests, the coupling frequency can be defined as $f_c = f_p - 2f_1$, where f_p is the frequency of the injected perturbation. This enables identical workflow for the post-processing of the measurements from both perturbation tests.

The elements of $\boldsymbol{Y}_{\mathrm{PN}}(s)$ are related as follows [21]:

$$Y_{\mathrm{pp}}(s) = Y_{\mathrm{nn}}(-s)^*$$

$$Y_{\mathrm{pn}}(s) = Y_{\mathrm{np}}(-s)^* \tag{10}$$

Using (4) and (10), the response of $\mathbf{Y}_{\mathrm{PN}}(s)$ at a complex frequency 's' can be used to obtain the response of $Y_p(s)$ and $Y_{\mathrm{cp}}(s)$ at frequencies $(s+j\omega_1)$ and $(-s+j\omega_1)$ as follows:

$$Y_p(s + j\omega_1) = Y_{\mathrm{pp}}(s)$$

$$Y_p(-s + j\omega_1) = Y_{\mathrm{nn}}(s)^* \tag{11}$$

and

$$Y_{\mathrm{cp}}(s + j\omega_1) = Y_{\mathrm{np}}(s)$$

$$Y_{\mathrm{cp}}(-s + j\omega_1) = Y_{\mathrm{pn}}(s)^* \tag{12}$$

Eq. (11) and (12) show that the measurement of $\mathbf{Y}_{\mathrm{PN}}(s)$ at positive frequencies gives the response of $Y_p(s)$ and $Y_{\mathrm{cp}}(s)$ at both positive and negative frequencies. The response of $Y_n(s)$ and $Y_{\mathrm{cn}}(s)$ at positive frequencies can be derived from the response of $Y_p(s)$ and $Y_{\mathrm{cp}}(s)$ at negative frequencies by using the following relationships [21]:

$$Y_n(s) = Y_p(-s)^*$$

$$Y_{\mathrm{cn}}(s) = Y_{\mathrm{cp}}(-s)^* \tag{13}$$

Hence, the response of the sequence admittance with frequency coupling can be completely described by the response of the positive-sequence direct and coupling admittances, $Y_p(s)$ and $Y_{\mathrm{cp}}(s)$, at both positive and negatives frequencies.

C. Response of SISO Sequence Admittance

Eq. (6) and (7) can be rewritten as follows:

$$Y_p(s + j\omega_1, Z_g) = Y_{\mathrm{pp}}(s) - \frac{Y_{\mathrm{pn}}(s)Y_{\mathrm{np}}(s) \cdot Z_g(s - j\omega_1)}{1 + Y_{\mathrm{nn}}(s) \cdot Z_g(s - j\omega_1)} \tag{14}$$

$$Y_n(s - j\omega_1, Z_g) = Y_{\mathrm{nn}}(s) - \frac{Y_{\mathrm{pn}}(s)Y_{\mathrm{np}}(s) \cdot Z_g(s + j\omega_1)}{1 + Y_{\mathrm{pp}}(s) \cdot Z_g(s + j\omega_1)} \tag{15}$$

Based on (14), the response of the grid-dependent, SISO, positive-sequence admittance, $Y_p(s, Z_g)$, can be obtained at the complex frequency $(s+j\omega_1)$ from the measured response of $\mathbf{Y}_{\mathrm{PN}}(s)$ at the complex frequency 's'; hence, the measurements of $\mathbf{Y}_{\mathrm{PN}}(s)$ can be used to derive the response of $Y_p(s, Z_g)$ at frequencies greater than 60 Hz. Similarly, it can be inferred from (15) that the response of $\mathbf{Y}_{\mathrm{PN}}(s)$ can be used to obtain the response of $Y_n(s, Z_g)$ at frequencies greater than –60 Hz. The response of $Y_p(s, Z_g)$ between 0 and 60 Hz can be obtained from the response of $Y_n(s, Z_g)$ between –60 and 0 Hz using (13); hence, the measurements of the MIMO sequence admittance $\mathbf{Y}_{\mathrm{PN}}(s)$ can be used along with the response of the grid impedance, $Z_g(s)$, to obtain the responses of the uncoupled positive- and negative-sequence SISO admittances, $Y_p(s, Z_g)$ and $Y_n(s, Z_g)$. Unlike [35], the proposed method achieves this without requiring different source/grid impedances for each perturbation test.

V. VALIDATION OF THE PROPOSED METHOD

The proposed method is validated using numerical simulations of a 2.5-MVA/0.69-kV, grid-connected, two-level VSC. The circuit diagram and control system of the VSC simulated in PSCAD are presented in our previous work [40]. The parameters of the simulated VSC are given in TABLE I. Python and MATLAB scripts are developed to automate the sequence admittance measurement process described in the flowchart shown in Fig. 3 [1]. The Python scripts interface with the PSCAD software and sequentially inject perturbations at different frequencies defined in the input frequency vector. The MATLAB scripts are used to post-process the voltage and currents measurements obtained during the perturbation tests and derive the sequence admittance response. Fig. 4 compares the measured response of the sequence admittance of the simulated VSC against predictions by the analytical model reported in [21]. Fig. 4 also demonstrates the importance of reference frame alignment in the sequence admittance measurement process. Previous works focussing on sequence impedance measurement failed to observe the impact of the sequence admittance reference frame because they performed measurements in simulations where the reference frame is unknowingly aligned with the grid voltage when the injected perturbation signals are generated using an internal simulation time reference that is also used to generate the grid voltages at the fundamental frequency.

Eq. (14) and (15) can be used to obtain the uncoupled SISO positive- and negative-sequence admittances of the VSC, depending on the impedance of the grid at its terminals, by using the measurements of the MIMO admittance, $\mathbf{Y}_{\mathrm{PN}}(s)$, obtained using the proposed method. Fig. 5 compares the SISO positive-sequence admittance, $Y_p(s, Z_g)$, of the VSC for a weak inductive grid at its terminals with the short-circuit ratio (SCR) of 2, obtained using (14) and the measurements of $\mathbf{Y}_{\mathrm{PN}}(s)$, against the response obtained by direct measurements. Figs. 4 and 5 validate the fundamental principles of the proposed method for measuring sequence admittance with frequency coupling.
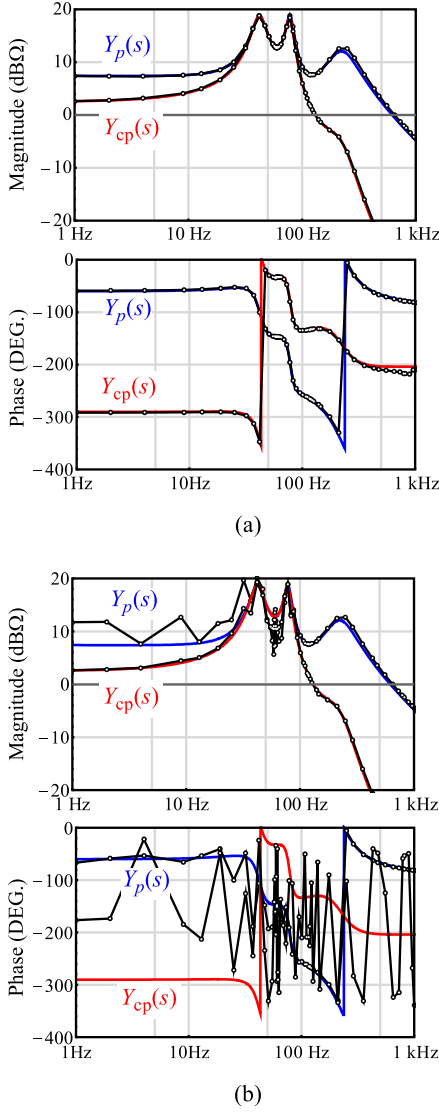
Fig. 4. Response of the positive-sequence admittance, $Y_p(s)$, and coupling admittance, $Y_{\mathrm{cp}}(s)$, of a 2.5-MVA grid-connected VSC simulated in PSCAD. The dots show the measurements obtained from simulations using the proposed method, and the solid lines show analytical model predictions. (a) The reference frame alignment algorithm is enabled; (b) the reference frame alignment algorithm is disabled.
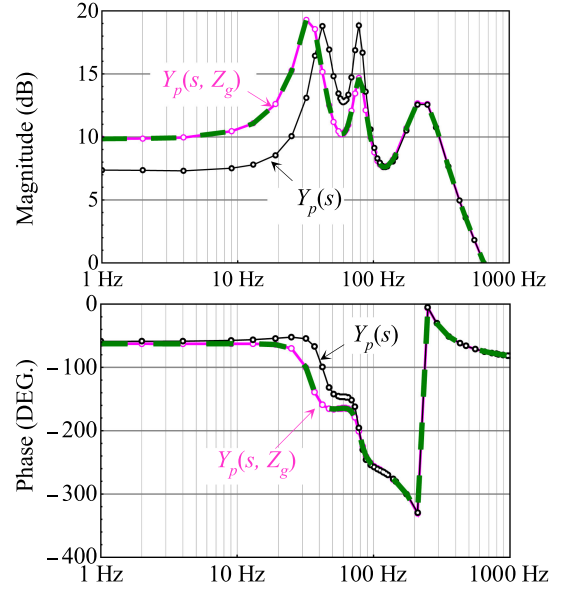

Fig. 5. The grid-dependent, SISO, positive-sequence admittance response of the 2.5-MVA VSC for a weak inductive grid with the SCR of 2 at its terminals. Black thin lines: response for an ideal grid; pink lines with circles: response for the weak inductive grid as derived from the measurements of $Y_{\mathrm{PN}}(s)$ and the grid impedance $Z_g(s)$; green dashed lines: direct measurements for the weak grid condition.
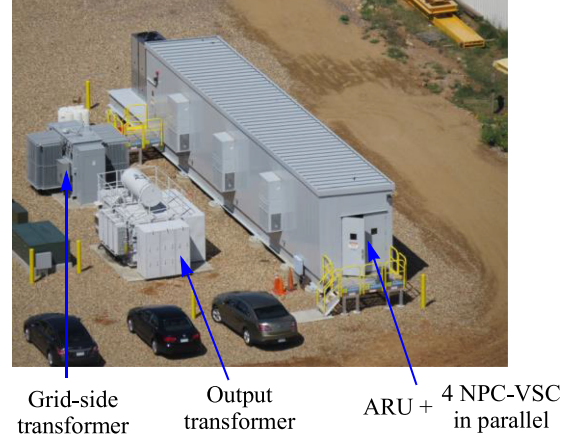

Fig. 6. 13.8-kV, 7-MVA grid simulator, called the CGI. Source: Mark McDade, NREL.

VI. ADMITTANCE MEASUREMENT OF A UTILITY-SCALE WIND TURBINE AND AN INVERTER USING A GRID SIMULATOR

This section demonstrates the sequence admittance measurement for a 1.9-MW wind turbine drivetrain and a 2.2-MVA inverter. The accuracy of the measurement system is verified by measuring the sequence admittance of a medium-voltage, low-pass harmonic filter whose parameters are known.

A. Measurement System

Fig. 6 shows the 13.8-kV/7-MVA grid simulator, the controllable grid interface (CGI), at the Flatirons Campus of the National Renewable Energy Laboratory (NREL) in Colorado, United States; it is configured to sequentially inject perturbations at different frequencies superimposed on nominal voltages at 60 Hz to measure the sequence admittance of the DUT. The CGI is custom designed based on ABB's ACS6000 medium-voltage drive technology. It features a 9-MVA active rectifier unit (ARU) at the utility side, which regulates the intermediate dc bus voltage. A controllable grid is established by four front-end, neutral-point-clamped voltage source converters (NPC-VSCs), each with a rated output of 3.3 kV, connected in parallel. A specialized multi-winding output transformer synthesizes 17-level voltage waveforms by combining the 3-level phase voltages from the NPC-VSCs and steps up the voltage to 13.8 kV.

Fig. 7 shows the schematic of the admittance measurement system. The CGI is controlled by a real-time digital simulator
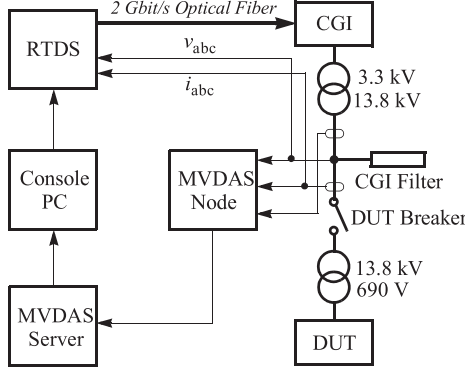
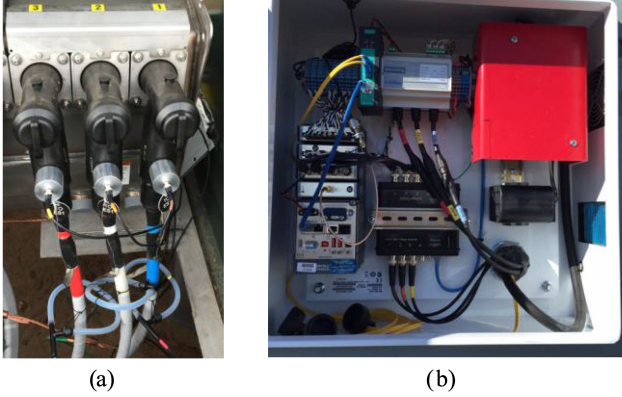Fig. 7. Schematic of the impedance measurement system at NREL.

(a)   (b)

Fig. 8. Hardware inside MVDAS sensing node: (a) voltage and current sensors; (b) data conditioning built around NI 9030 cRIO platform. Source: NREL.

Fig. 9. 5-MW dynamometer. Source: Dennis Schroeder, NREL.

TABLE II
SYSTEM PARAMETERS

Parameter	Value
7 MW Grid Simulator (CGI)	
Rated Voltage	13.8 kV
Equivalent Switching Frequency	4320 Hz
Control System Sampling Time	250 μs
1.9-MW Type III Wind Turbine Drivetrain	
Induction Generator Rated Speed	1500 rpm
Number of Poles	6
Rated Voltage	690 V
CGI Filter	
Filter Resistance, R_f	15 Ω
Filter Capacitance, C_f	6.39 μF

(RTDS) using a fast 2-Gbit/s optical fiber interface, and it receives voltage reference signals over the optical fiber every 25 μs; however, the equivalent switching frequency of the CGI and the sampling time of its control system limit the maximum frequency of the perturbations to 2 kHz. As shown in Fig. 7, a custom-designed, medium-voltage data acquisition system (MVDAS) node is used to obtain the GPS-synchronized measurements of the three-phase voltages and currents at the terminals of the DUT at 50-kHz sampling frequency. Fig. 8 shows the hardware inside the MVDAS node, which includes capacitive voltage sensors [41], Rogowski-coil-based current sensors [42], and a GPS-synchronized signal conditioning unit built around the National Instruments (NI) 9030 cRIO platform. Ten seconds of voltage and current waveforms are captured for each perturbation test and stored locally for post-event downloading, reference-frame alignment, and FFT analysis.

Fig. 9 shows the 5-MW dynamometer at NREL that is used for the admittance measurement of wind turbine drivetrains. To measure the admittance at a specific operation point, the dynamometer operates the drivetrain at a desired speed, and the turbine control system sets its active and reactive power output.

The entire sequence admittance measurement process described in Fig. 3 is automated using MATLAB software on a console PC, as shown in Fig. 7. Initialization inputs to the system include a v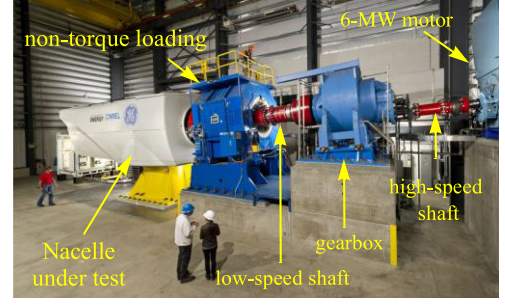ector with frequency points where the sequence admittance matrix, $\mathbf{Y}_{PN}(s)$, needs to be measured and another vector with the magnitudes of the voltage perturbations to be injected for different perturbation frequencies.

Table II shows the key parameters of the grid simulator, a series RC harmonic filter connected at the terminals of the grid simulator, and the 1.9-MW wind turbine drivetrain.

B. CGI Filter

This section demonstrates the sequence admittance measurement of the CGI filter, by keeping the DUT breaker open (refer Fig. 7), to verify the accuracy of the admittance measurement system. The positive- and negative-sequence admittances of the filter can be written as:

$$Y_p(s) = Y_n(s) = \left\{ R_f + \frac{1}{sC_f} \right\}^{-1} \qquad (16)$$

Note that the coupling admittances, $Y_{cp}(s)$ and $Y_{cn}(s)$, are zero for the filter. Fig. 10 compares the measured responses of $Y_p(s)$ and $Y_{cp}(s)$ with the analytical prediction; the measured response of $Y_p(s)$ exactly matches the prediction using (16), and as expected, the coupling part of the sequence admittance, $Y_{cp}(s)$, is practically zero at all frequencies.
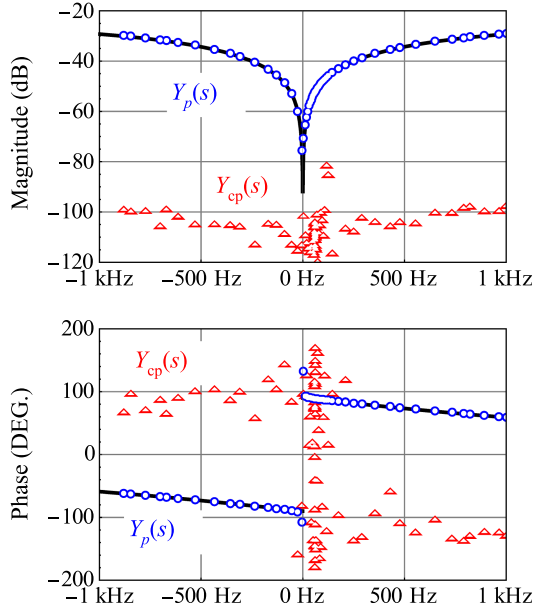
Fig. 10. Sequence admittance, $Y_p(s)$ and $Y_{cp}(s)$, of a three-phase RC filter connected at the terminals of the 13.8-kV/7-MVA grid simulator. Black thick lines: analytical model predictions; circles and triangles: measurements of $Y_p(s)$ and $Y_{cp}(s)$, respectively.
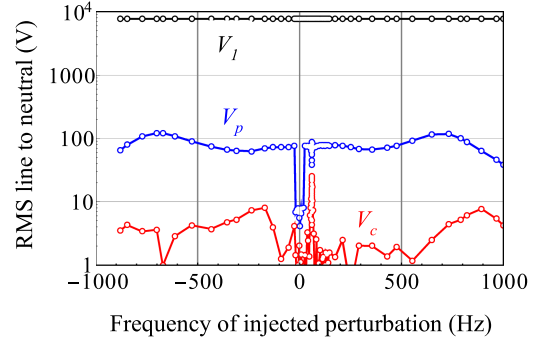

Fig. 11. Magnitude of the frequency components in the voltages at the terminals of a 1.9-MW wind turbine drivetrain during the injection of positive-sequence perturbations. V_1: fundamental frequency (f_1) component; V_p: perturbation frequency (f_p) component; and V_c: coupling frequency ($f_c = f_p-2f_1$) component.
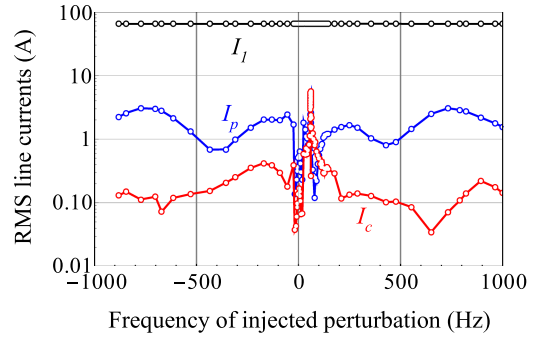

Fig. 12. Magnitude of the frequency components in the output currents of a 1.9-MW wind turbine drivetrain during the injection of positive-sequence perturbations. I_1: fundamental frequency (f_1) component; I_p: perturbation frequency (f_p) component; and I_c: coupling frequency ($f_c = f_p-2f_1$) component.

C. 1.9-MW Wind Turbine Drivetrain

The sequence admittance of the 1.9-MW/0.69-kV Type III wind turbine drivetrain—including a front-end transformer that steps up the turbine voltage to 13.8 kV—was measured for a specific operation point: The drivetrain was operated at 1,490 rpm, and it was configured to deliver the power output of 1.5 MW and 0 MVAR to the CGI. The synchronous speed of the wind turbine, calculated using the number of poles of the induction generator from Table II, is 1,200 rpm; hence, 1,490 rpm represents super-synchronous operation and the slip of –0.24. Note that the admittance of the wind turbine will be different for different operation speeds and power levels.

The sequence admittance matrix, $\mathbf{Y}_{PN}(s)$, of the turbine is measured at frequency points between 0.1 and 940 Hz. Based on the flowchart shown in Fig. 3, this requires the injection of positive-sequence perturbations at frequencies ranging from –880 Hz ($= -940+60$) to 1,000 Hz ($= +940+60$). Note again that the injection of positive-sequence perturbations at negative frequencies is equivalent to the injection of negative-sequence perturbations at positive frequencies. The admittance of Type III wind turbines is very high at low frequencies because it is dominated by the leakage inductance of the generator; hence, the magnitude of the injected voltage perturbation is reduced for perturbation frequencies between –20 and +20 Hz to avoid the current response from becoming too high to violate the small-signal condition or trigger an overcurrent protection and trip the wind turbine. Fig. 11 shows the magnitude of different frequency components in three-phase voltages (line to neutral) at the terminals of the drivetrain for each perturbation test. Note that the fundamental frequency component is maintained at 7.9 kV; the perturbation and coupling frequency components are

small enough to ensure small-signal perturbation condition; and the coupling frequency component is non-negligible around the fundamental frequency—signifying strong frequency coupling. Fig. 12 similarly shows different frequency components in the output currents of the wind turbine drivetrain. Note that the coupling frequency response in the currents is higher than the perturbation frequency response around the fundamental frequency; this creates a coupling frequency component in voltages depending on the impedance of the source—in this case, the 7-MVA grid simulator.

Fig. 13 shows the measured response of $\mathbf{Y}_{PN}(s)$. Based on the discussion in the previous section, the measurements of $\mathbf{Y}_{PN}(s)$ from 0.1 to 940 Hz can be used to derive the response of $Y_p(s)$ and $Y_{cp}(s)$ from –880 to +1,000 Hz. The responses of $Y_p(s)$ and $Y_{cp}(s)$ derived from the measurements of $\mathbf{Y}_{PN}(s)$ are shown in Fig. 14; the responses are shown only for the positive frequencies for clarity. Both Figs. 13 and 14 show the presence of significant frequency coupling at frequencies less than 200 Hz; in fact, at certain frequencies, the coupling admittance $Y_{cp}(s)$ is higher than the direct admittance $Y_p(s)$. This demonstrates the importance of using the sequence admittance with frequency coupling for the analysis of low-frequency control interaction and resonance problems.
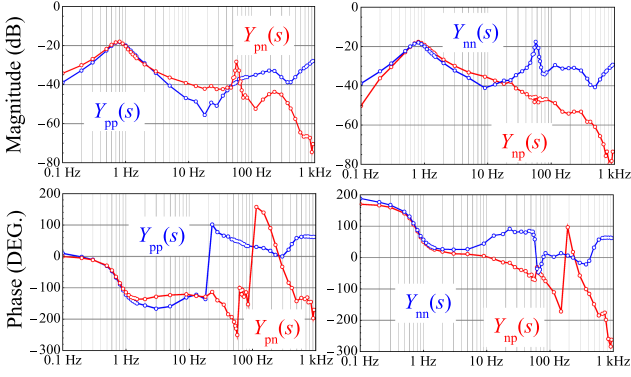
Fig. 13. Measured response of the sequence admittance matrix, $Y_{PN}(s)$, of a 1.9-MW, 0.69-kV Type III wind turbine drivetrain.
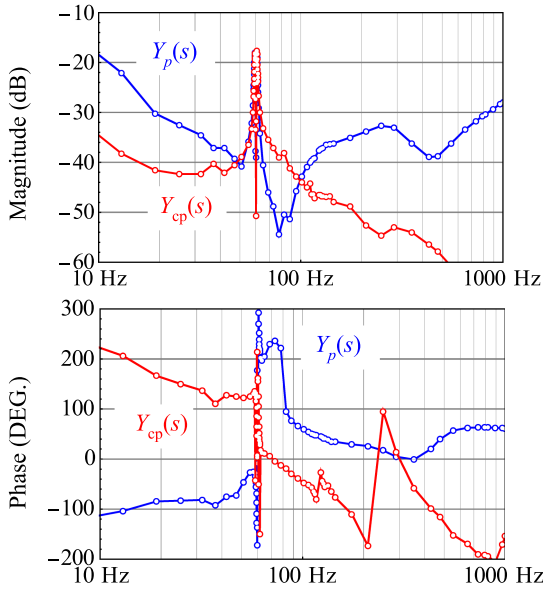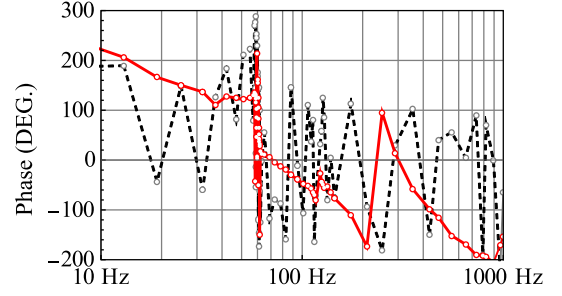

Fig. 15. Phase response of the coupling part, $Y_{cp}(s)$, of the sequence admittance of a 1.9-MW wind turbine drivetrain. Solid red lines: with reference frame alignment algorithm enabled. Dashed black lines: with reference frame alignment algorithm disabled.
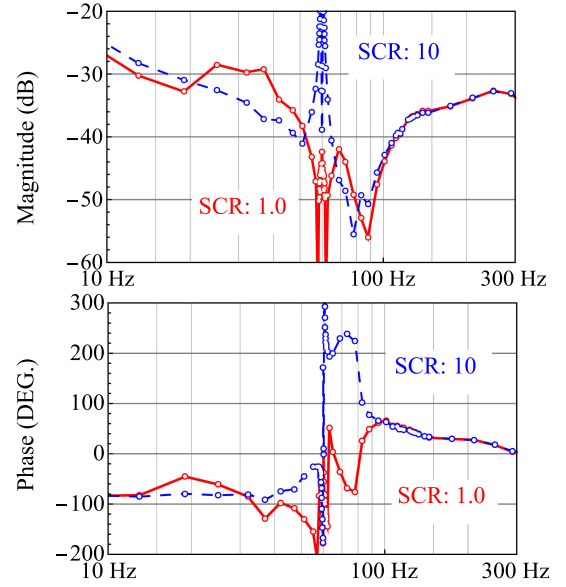

Fig. 14. Measurement of the positive-sequence direct admittance, $Y_p(s)$, and the coupling admittance, $Y_{cp}(s)$, of a 1.9-MW Type III wind turbine drivetrain.

Fig. 16. Positive-sequence SISO admittance, $Y_p(s, Z_g)$, of a 1.9-MW Type III wind turbine for two different grid conditions obtained from the measurements of the sequence admittance matrix, $Y_{PN}(s)$, and the grid impedance, $Z_g(s)$.

Fig. 15 experimentally shows the importance of aligning the sequence admittance reference frame. It compares the phase response of the coupling admittance, $Y_{cp}(s)$, with and without aligning the reference frame using the proposed algorithm. Clearly, the phase response obtained without aligning the reference frame does not provide any meaningful information.

Fig. 16 shows for two different grid conditions the grid-dependent response of the uncoupled SISO positive-sequence admittance, $Y_p(s, Z_g)$, of the 1.9-MW turbine obtained using (14) and the measured response of $Y_{PN}(s)$. An inductive grid is assumed to obtain these responses, and the corresponding grid inductance is obtained based on the SCR indicated in the figure. The response of $Y_p(s, Z_g)$ is the same as the response of $Y_p(s)$ for a strong grid condition; however, it changes significantly as the grid becomes weaker. Note that the conventional positive-sequence admittance, $Y_p(s)$, does not account for the frequency coupling, whereas the grid-dependent SISO positive-sequence admittance, $Y_p(s, Z_g)$, captures the frequency coupling in its response.

To experimentally demonstrate the equivalence between the dq admittance and the sequence admittance, the dq admittance response of the 1.9-MW turbine is measured using the method presented in [15], and it is compared with the dq admittance response obtained from the sequence measurements shown in Fig. 13 using the relationship between the dq and sequence admittances reported in [21]. Fig. 17 shows this comparison and verifies the relationship between the two approaches of representing three-phase power systems.

D. Impact of Fundamental Frequency on Accuracy

It is possible to maintain the fundamental frequency precisely at 60 Hz when a grid simulator facility, such as the one presented in this paper, is used to perform the admittance measurement tests; however, this cannot be ensured when the DUT is connected to a utility grid and a series- or shunt-connected perturbation source is used to measure the sequence admittance. Fundamental frequency different from 60 Hz can introduce
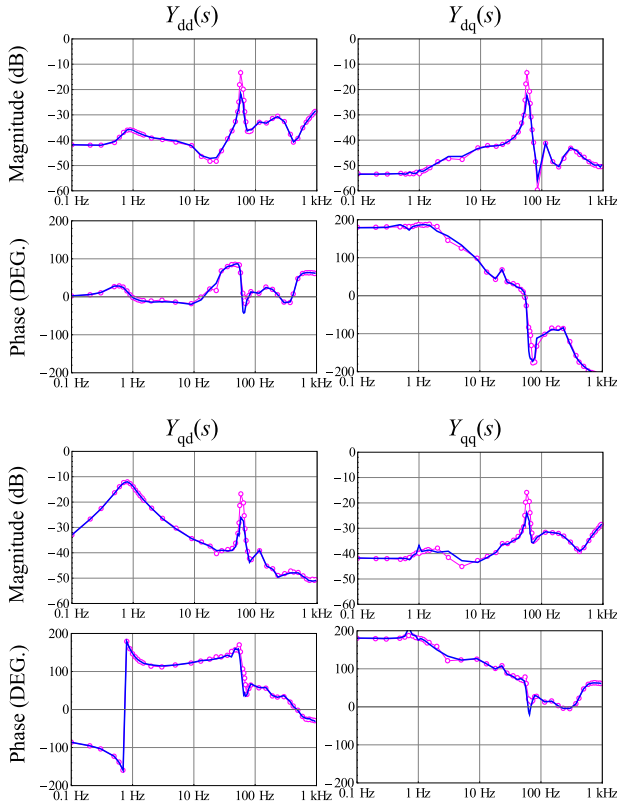
Fig. 17. Comparison of the response of the dq admittance matrix, $Y_{DQ}(s)$, of a 1.9-MW Type III wind turbine drivetrain obtained from the measurements of its sequence admittance matrix, $Y_{PN}(s)$, (shown by blue lines) against the direct measurement of the dq admittance matrix (shown by pink circles).
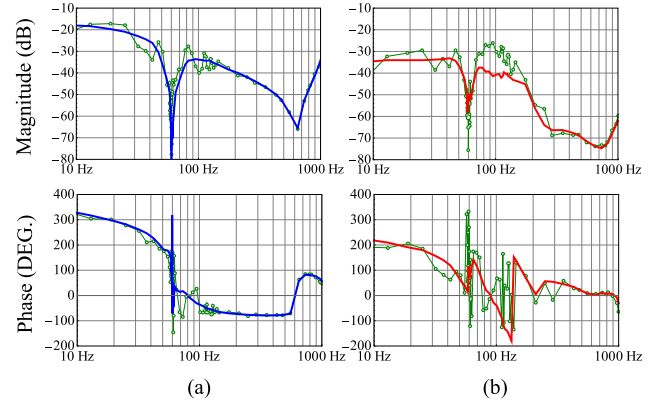

Fig. 18. Sequence admittance measurements of a 2.2-MWVA inverter when the fundamental frequency is 60 Hz (solid lines) and when it is 59.87 Hz (lines with circles). (a) Positive-sequence admittance, $Y_p(s)$; (b) coupling admittance, $Y_{cp}(s)$.

in the sequence admittance measurement when the fundamental frequency is different from 60 Hz and/or time-varying will be explored in a future work.

VII. CONCLUSION

This paper presented a method for measuring the sequence admittance of three-phase electrical systems exhibiting frequency coupling effects such as wind turbines, inverters, synchronous generators, induction generators, HVDC converters, and power system networks with these active devices. The paper also compared different aspects of the sequence and dq admittance measurement processes. It showed that the sequence admittance has a reference frame similar to the dq admittance, and it should be aligned with the grid voltage angle for the accurate measurement of the sequence admittance response. An algorithm for aligning the sequence admittance reference frame based on the estimation of the grid voltage angle is presented in the paper. The paper also demonstrated the impact of the value of the fundamental frequency during testing on the accuracy of the sequence admittance measurements. The proposed measurement method can obtain the sequence admittance response in both MIMO and SISO forms. The proposed sequence admittance measurement method and the practical issues associated with the impedance measurement of utility-scale wind turbines and inverters are demonstrated by measuring the sequence admittance of a 1.9-MW Type III wind turbine drivetrain and a 2.2-MVA inverter using an impedance measurement system built around a 7-MVA grid simulator and a 5-MW dynamometer.

errors in admittance measurements through several paths: (1) when the length of the data window used for the FFT analysis does not contain an integral number of cycles of the fundamental, perturbation, and coupling frequency components, it will result in spectral leakage and cause errors in the measurements; (2) a non-nominal fundamental frequency that is not known can cause significant errors in the estimation of the grid voltage angle if the FFT-based method is employed assuming that the fundamental frequency is fixed at its nominal value. This will result in an incorrect alignment of the Fourier components with the grid voltage angle and cause errors in the admittance measurements. Fig. 18 shows the impact of the fundamental frequency on the sequence admittance measurements of a 2.2-MVA inverter at the front end of a 1-MW/1-MWh battery energy storage system at the Flatirons Campus of NREL. The figure shows the admittance measurements when the fundamental frequency is set at 60 Hz and 59.87 Hz, respectively, by the CGI. Clearly, the measurement accuracy suffers significantly when the fundamental frequency is different from 60 Hz and the measurement process assumes it to be at 60 Hz.

The errors in the grid voltage angle estimation can be mitigated by measuring the fundamental frequency during sequence admittance measurements, for example, by using a PLL. Moreover, the measurement errors because of the spectral leakage can be minimized by using appropriate window functions [43]. The use of a PLL and different window functions to mitigate errors

REFERENCES

[1] S. Shah, P. Koralewicz, V. Gevorgian, H. Liu, and J. Fu, "Impedance methods for analyzing the stability impacts of inverter-based resources—stability analysis tools for modern power systems," *IEEE Electrific. Mag.*, vol. 9, no. 1, pp. 53–65, Mar. 2021, doi: 10.1109/MELE.2020.3047166.

[2] "Wind energy systems sub-synchronous oscillations: events and modeling," *IEEE Power Energy Soc.* Tech. Rep., PES-TR80, Jul. 2020.

[3] C. Buchhagen, C. Rauscher, A. Menze, and J. Jung, "BorWin1 - first experiences with harmonic interactions in converter dominated grids," in *Proc. Int. ETG Congr.*, Bonn, Germany, 2015, pp. 27–33.

[4] E. Mollerstedt and B. Bernhardsson, "Out of control because of harmonics—An analysis of the harmonic response of an inverter locomotive," *IEEE Control Syst. Mag.*, vol. 20, no. 4, pp. 70–81, Aug. 2000.

[5] D. Shu, X. Xie, H. Rao, X. Gao, Q. Jiang, and Y. Huang, "Sub- and super- synchronous interactions between STATCOMs and weak AC/DC transmissions with series compensations," *IEEE Trans. Power Electron.*, vol. 33, no. 9, pp. 7424–7437, Nov. 2017.

[6] L. C. Gross, "Sub-synchronous grid conditions: New event, new problem, and new solutions," in *Proc. Western Protective Relay Conf.*, Spokane, WA, 2010, pp. 1–19.

[7] H. Liu, X. Xie, X. Gao, H. Liu, and Y. Li, "Stability analysis of SSR in multiple wind farms connected to series-compensated systems using impedance network model," *IEEE Trans. Power Syst.*, vol. 33, no. 3, pp. 3118–3128, May 2018.

[8] L. Kocewiak *et al.*, "Overview, status, and outline of stability analysis in converter-based power systems," in *Proc. Virtual Wind Integr. Workshop*, Nov. 2020, p. 10.

[9] E. Rehman, M. G. Miller, J. Schmall, S. H. Huang, and J. Billo, "Stability assessment of high penetration of inverter-based generation in the ERCOT grid," in *Proc. IEEE Power Energy Soc. Gen. Meeting*, Atlanta, GA, USA, 2019, pp. 1–5.

[10] A. Dissanayaka, J. Wiebe, and A. Isaacs, "Panhandle and South Texas stability and system strength assessment," *Electranix*, Winnipeg, MB, Canada, 2018.

[11] *Power System Model Guidelines*. Melbourne, Australia: Australian Energy Market Operator, 2018.

[12] M. Belkhayat, "Stability criteria for AC power systems with regulated loads," Ph.D. dissertation, Dept. Elect. Eng., Purdue Univ., West Lafayette, IN, USA, Dec. 1997.

[13] Y. A. Familiant, J. Huang, K. A. Corzine, and M. Belkhayat, "New techniques for measuring impedance characteristics of three-phase AC power systems," *IEEE Trans. Power Electron.*, vol. 24, no. 7, pp. 1802–1810, Jul. 2009.

[14] J. Huang, K. A. Corzine, and M. Belkhayat, "Small-signal impedance measurement of power-electronics-based AC power systems using line-to-line current injection," *IEEE Trans. Power Electron.*, vol. 24, no. 2, pp. 445–455, Feb. 2009.

[15] M. Jaksic *et al.*, "Medium-voltage impedance measurement unit for assessing the system stability of electric ships," *IEEE Trans. Energy Conv.*, vol. 32, no. 2, pp. 829–841, Jun. 2017.

[16] G. Francis, "An algorithm and system for measuring impedance in D-Q coordinates," Ph.D. dissertation, Dept. Elect. Eng., Virgina Polytechnic Institute and State University, Blacksburg, VA, 2010.

[17] Z. Shen *et al.*, "Analysis of phase locked loop (PLL) influence on dq impedance measurement in three-phase ac systems," in *Proc. Appl. Power Electron. Conf. Expo.*, Long Beach, CA, USA, 2013, pp. 939–945,.

[18] H. Gong, D. Yang, and X. Wang, "Impact analysis and mitigation of synchronization dynamics for dq impedance measurement," *IEEE Trans. Power Electron.*, vol. 34, no. 9, pp. 8797–8807, Sep. 2019.

[19] J. Sun, "Small-signal methods for AC distributed power systems—A review," *IEEE Trans. Power Electron.*, vol. 24, no. 11, pp. 2545–2554, Nov. 2009.

[20] M. Cespedes and J. Sun, "Impedance modeling and analysis of grid-connected voltage-source converters" *IEEE Trans. Power Electron.*, vol. 29, no. 3, pp. 1254–1261, Mar. 2014.

[21] S. Shah and L. Parsa, "Impedance modeling of three-phase voltage source converters in DQ, sequence, and phasor domains," *IEEE Trans. Energy Conv.*, vol. 32, no. 3, pp. 1139–1150, Apr. 2017.

[22] S. Shah and L. Parsa, "Sequence-domain transfer matrix model of three-phase voltage source converters," in *Proc. IEEE Power Energy Soc. General Meeting*, Boston, MA, USA, 2016, p. 5.

[23] A. Rygg, M. Molinas, C. Zhang, and X. Cai, "A modified sequence-domain impedance definition and its equivalent to the DQ-domain impedance definition for the stability analysis of AC power electronic systems," *IEEE J. Emerg. Sel. Topics Power Electron.*, vol. 4, no. 4, pp. 1383–1396, Dec. 2016.

[24] M. K. Bakhshizadeh *et al.*, "Couplings in phase domain impedance modeling of grid-connected converters," *IEEE Trans. Power Electron.*, vol. 31, no. 10, pp. 6792–6796, Oct. 2016.

[25] W. Ren and E. Larsen, "A refined frequency scan approach to sub-synchronous control interaction (SSCI) study of wind farms," *IEEE Trans. Power Syst.*, vol. 31, no. 5, pp. 3904–3912, Sep. 2016.

[26] X. Zhang, S. Fu, W. Chen, N. Zhao, G. Wang, and D. Xu, "A symmetrical control method for grid-connected converters to supress the frequency coupling under weak grid conditions," *IEEE Trans. Power Electron.*, vol. 35, no. 12, pp. 13488–13499, Dec. 2020.

[27] S. Shah, P. Koralewicz, V. Gevorgian, and L. Parsa, "Small-signal modeling and design of phase-locked loops using harmonic signal-flow graphs," *IEEE Trans. Energy Conv.*, vol. 35, no. 2, pp. 600–610, Jun. 2020.

[28] S. Shah, "Impedance of three-phase systems in DQ, sequence, and phasor domains," *IEEE Power and Energy Soc. Publications Webinar Series*, Aug. 2020. Accessed: Jul. 14, 2021. [Online]. Available: https://ieeetv.ieee.org/ondemand/impedance-of-three-phase-systems-in-dq-sequence-and-phasor-domains

[29] H. Li, H. Guo, J. Liang, and L. Qi, "Impedance-based stability analysis of MVDC systems using generator-thyristor units and DTC motor drives," *IEEE J. Emerg. Sel. Topics Power Electron.*, vol. 5, no. 1, pp. 5–13, Mar. 2017.

[30] S. Shah, P. Koralewicz, V. Gevorgian, and R. Wallen, "Impedance measurement of wind turbines using a multimegawatt grid simulator," in *Proc. 18th Wind Integr. Workshop*, Dublin, Ireland, 2019, p. 6.

[31] S. Shah, P. Koralewicz, V. Gevorgian, and R. Wallen, "Impedance characterization of utility-scale renewable and energy storage systems," in *Proc. IEEE Energy Conv. Cong. Expo.*, Baltimore, MD, USA, 2019, pp. 2609–2616.

[32] M. Cespedes and J. Sun, "Three-phase impedance measurement for system stability analysis," in *Proc. IEEE 14th Workshop Control Modeling Power Electron. (COMPEL)*, Salt Lake City, UT, USA, 2013, p. 6.

[33] W. Cao, Y. Ma, and F. Wang, "Sequence-impedance-based harmonic stability analysis and controller parameter design of three-phase inverter-based multibus AC power systems," *IEEE Trans. Power Electron.*, vol. 32, no. 10, pp. 7674–7693, Oct. 2017.

[34] T. Roinila, H. Abdollahi, and E. Santi, "Frequency-domain identification based on pseudorandom sequences in analysis and control of DC power distribution systems: A review," *IEEE Trans. Power Electron.*, vol. 36, no. 4, pp. 3744–3756, Apr. 2021.

[35] J. Liu, X. Du, Y. Shi, and H.-M. Tai, "Impedance measurement of three-phase inverter in the stationary frame using frequency response analyzer," *IEEE Trans. Power Electron.*, vol. 35, no. 9, pp. 9390–9401, Sep. 2020.

[36] Y. Liao and X. Wang, "Stationary-frame complex-valued frequency-domain modeling of three-phase power converters," *IEEE J. Emerg. Sel. Topics Power Electron.*, vol. 8, no. 2, pp. 1922–1933, Jun. 2020.

[37] T. Reinikka, T. Roinila, and J. Sun, "Measurement device for inverter output impedance considering the coupling over frequency," in *Proc. IEEE 21st Workshop Control Modeling Power Electron.*, Aalborg, Denmark, 2020, p. 7.

[38] T. Reinikka, T. Roinila, and J. Sun, "Accurate measurement of converter sequence impedance by active cancellation of coupling over frequency," in *Proc. 2019 4th IEEE Workshop Electronic Grid (eGRID)*, Xiamen, China, 2019, p. 6.

[39] I. Vieto and J. Sun, "On system modeling and analysis using DQ-frame impedance models," in *Proc. IEEE 18th Workshop Control Modeling Power Electron.*, Stanford, CA, USA, 2017, p. 8.

[40] S. Shah *et al.*, "Large-signal impedance-based modeling and mitigation of resonance of converter-grid systems," *IEEE Trans. Sustain. Energy*, vol. 10, no. 3, pp. 1439–1449, Jul. 2019.

[41] Jomitek – Powerful Solutions, "The Jomitek v3 voltage sensor," Datasheet, 2012.

[42] Powertek - RCTi current sensors, "RCTi single-phase current transducer," Datasheet. Accessed: Jul. 17, 2019. [Online]. Available: www.powertekuk.com/rcti-single-phase-current-transducer.pdf

[43] E. Louarroudi, R. Pintelon, and J. Lataire, "Accurate frequency domain measurement of the best linear time-invariant approximation of linear time-periodic systems including the quantification of the time-periodic systems," *ELSEVIER Mech. Syst. Signal Process.*, vol. 48, pp. 274–299, 2014.

Shahil Shah (Senior Member, IEEE) received the B.E. degree in electrical engineering from Government Engineering College, Gandhinagar, India, in 2006, the M.Tech. degree in electrical engineering from the Indian Institute of Technology Kanpur, Kanpur, India, in 2008, and the Ph.D. degree in electrical engineering from Rensselaer Polytechnic Institute (RPI), Troy, NY, USA, in 2018. He is currently a Senior Engineer with Power Systems Engineering Center, National Renewable Energy Laboratory, Golden, CO, USA. His research interests include dynamic and transient stability of renewable energy systems and power systems with high levels of inverter-based resources. He is an associate editor of the IEEE TRANSACTIONS ON ENERGY CONVERSION. Dr. Shah was the recipient of the 2018 RPI Allen B. Dumont Prize, given to a doctoral candidate, who demonstrates high scholastic ability and makes substantial contribution to his/her field.

Przemyslaw Koralewicz (Member, IEEE) received the M.S.E.E. degree from Silesian Technical University, Gliwice, Poland, in 2010. He specializes in modeling, detailed analysis, and testing of smart inverters and complex power systems, including microgrids. He is utilizing the NREL Controllable Grid Interface (CGI), a new, groundbreaking testing apparatus and methodology to test and demonstrate many existing and future advanced controls for various renewable generation technologies on multimegawatt scale and medium-voltage levels.

Vahan Gevorgian (Senior Member, IEEE) received the Ph.D. degree in electrical engineering from the State Engineering University of Armenia, Yerevan, Armenia, in 1993. In October 1994, he joined National Renewable Energy Laboratory (NERL) and has served many roles over the years. He is currently with Power Systems Engineering Center, focused on renewable energy impacts on transmission and interconnection issues and dynamic modeling of variable generation systems. He is involved in many different areas, including the dynamometer and field testing of large and small wind turbines, dynamometer testing of wind turbine drivetrain components, development of advanced data acquisition systems, and wind turbine power quality. He provides technical support to NREL industry partners and main U.S. wind turbine manufacturers. He is a Member of the IEC team for wind turbine power quality standards. His contributions to NREL research have been recognized through multiple Outstanding Individual and Team Staff Awards.

Robb Wallen received the B.S. degree in electrical engineering from the University of Colorado, Boulder, CO, USA. Since 2009, he has been a Senior Engineer with National Renewable Energy Laboratory, working on the design and implementation of control and data acquisition systems. He is currently responsible for operating the National Wind Technology Center's 2.5 MW dynamometer, 5 MW dynamometer, and Controllable Grid Interface (CGI) facilities. He has more than 19 years of experience in the field of test engineering, system design, and large-scale test facility operation.